# Precision inhibitory stimulation of individual-specific cortical hubs slows information processing in humans

*Charles J. Lynch[1], Andrew L. Breeden[1], Evan M. Gordon[2], Joseph B. C. Cherry[1], Peter E. Turkeltaub[3,4], Chandan J. Vaidya[1,6]*

*[1]Department of Psychology, Georgetown University, [2]VISN 17 Center of Excellence for Research on Returning War Veterans, [3]Neurology Department, Georgetown University Medical Center, Children's Research Institute, [4]Neurology Department, Georgetown University Medical Center, Children's Research Institute,[5]Research Division, MedStar National Rehabilitation Hospital, [6]Children's National Medical Center, Washington DC*

Acknowledgements: This work was supported by Dean Toulmin's Pilot Project Award from Georgetown University Medical Center to P.E.T and C.J.V. We would like to thank the research staff at the Center for Functional and Molecular Imaging and Junaid Merchant for their assistance with data collection.

Addresses for correspondence:

Charles J. Lynch
306 White-Gravenor
Department of Psychology
Georgetown University, Washington, DC 20057
Email: cl968@georgetown.edu

Chandan J. Vaidya
306 White-Gravenor
Department of Psychology
Georgetown University, Washington, DC 20057
Email: cjv2@georgetown.edu

## Abstract

Non-invasive brain stimulation is a promising treatment for psychiatric and neurologic conditions, but outcomes are variable across treated individuals. This variability may be due in part to uncertainty regarding an optimal stimulation site – a challenge that may be complicated further by the variable organization of individual brains. Utilizing a network science framework, we predicted that stimulating "hubs" would have the greatest effect on cognition. First, using a publically available dataset, we discovered that different areas of cortex function as hubs in different individuals, but that hubs could be mapped reliably within an individual. We next used a prospective within-subjects double-blind design to demonstrate that inhibiting individual-specific hubs with transcranial magnetic stimulation disrupts information processing during working-memory, more so than inhibiting nearby non-hubs. Finally, hubs could be retrospectively clustered into subtypes that yielded different outcomes when inhibited. Based on these findings, we propose stimulating hub subtypes relevant for patient symptomatology as an intervention strategy.

## Introduction

There is widespread interest in utilizing non-invasive brain stimulation (NIBS) as a treatment for psychiatric and neurologic conditions [1], including addiction [2, 3], obsessive compulsive disorder [4], eating disorders [5], stroke [6], and depression [7, 8]. The outcomes of these interventions, however, are variable across treated individuals. In the most widely adopted, Federal Drug Administration approved application of NIBS – repetitive transcranial magnetic stimulation (TMS) for the treatment of medication refractory major depression – only 29% percent of patients respond positively [9]. Variability in patient response has been attributed in part to uncertainty regarding free parameters inherent to NIBS, including the stimulation site. Because the effects of NIBS are believed to propagate from the stimulation site in a manner constrained by the connectivity of the targeted brain area [10], appropriate stimulation site selection is likely critical for therapeutic success, as it will determine whether or not stimulation effects spread throughout clinically-relevant neural circuitry.

Strategies for selecting stimulation sites have largely focused upon anatomical landmarks [11, 12] and local tissue properties [13]. The same anatomical area, however, can exhibit unique patterns of connectivity in different individuals [14-17]. Thus, NIBS administered to the same anatomical area in different individuals may in practice target cortical areas serving different functional roles. The advent of specialized techniques for precisely characterizing the functional areal [18, 19] and network organization [15, 16, 20] of individual brains has set the stage for the development of personalized NIBS protocols. In principle, such an approach could reduce the variability introduced by selecting targets using traditional strategies, thus increasing the likelihood of positive clinical outcomes.

Because the effects of NIBS are in part non-local [10], a network-centric framework in which brain areas ("nodes") engage in networked communication within and across networks ("modules") [21], is well-suited for identifying cortical areas where the effects of NIBS on cognition may be most pronounced. In many complex physical [22] and biological networks [23] select nodes, termed hubs, serve outsized roles due to their participation in multiple network modules. Brain areas with hub-like properties have been identified using resting-state functional magnetic resonance imaging (rsfMRI) [24, 25], and are thought to serve critical roles in cognitive function and behavior [26, 27]. We predicted that administering NIBS to hubs would have a greater effect on cognition and behavior than non-hubs. If this prediction is borne out, it would

implicate hubs as compelling candidate targets in NIBS interventions for psychiatric and neurologic conditions, especially those exhibiting distributed network pathologies [28].

We first assessed the feasibility of mapping hubs using rsfMRI in individuals, and employing them as NIBS targets using the Midnight Scan Club (MSC) [17], a publically available dataset of highly-sampled individuals. We discovered that the spatial distribution of hub estimates was variable amongst individuals, and not represented accurately by a group-average. Furthermore, hub estimates were unreliable within an individual when using typical quantities of per-individual data. We developed an approach that solved both of these challenges, allowing for accurate and reliable mapping of hubs in individuals for the first time.

In a first of its kind experiment, we mapped cortical areas functioning as hubs on an individual-basis in twenty-four healthy participants. We predicted that administering an inhibitory form of patterned TMS to hubs would give rise to slower, less effective information processing during the performance of a cognitive task, relative to inhibition of nearby non-hub brain areas. To test this prediction, we fit a drift diffusion model to each participant's performance on an N-back task [29] following hub and non-hub inhibitory stimulation (administered in counter-balanced order in sessions >24 hrs. apart). We selected the N-back task, which requires the temporary maintenance and manipulation of information, as it involves component processes disrupted in many psychiatric and neurologic conditions, making it well-suited as a test-case in healthy individuals. The search space for TMS targets was constrained to right middle frontal gyrus, to ensure that both stimulation sites were in a region known to be relevant for N-back performance [30].

## Results

### *Hubs are unique to individuals*

We estimated the degree to which parcels of cortex in the right middle frontal gyrus of each MSC participant function as hubs using the graph theory metric, participation coefficient [31] (**Figure1b**). Each participant's entire 5-hr. rsfMRI dataset was used for this analysis. Parcels with higher participation coefficient values ("hubs") participate in more brain networks than those with lower values ("non-hubs") (**Figure1a**). Pairwise rank spatial correlations revealed that the spatial distribution of participation coefficients amongst individuals was not similar (**Figure1c**: avg. $r_s$ = -0.01 ± 0.26). Spatial correlations between participation coefficients defined in individuals and those from a group-average were higher (**Figure1c**: avg. $r_s$ = 0.09 ± 0.21), albeit only modestly.

The average distance between the Talairach coordinates corresponding to the centroid of the most hub-like parcel in each individual was 33 ± 21mm (**Figure1d**). Administering TMS to the group-average hub would have successfully stimulated the most hub-like parcel in at most 30% of MSC participants (**Figure1e**), assuming an effective spatial resolution of 0.5-2cm [32-34]. The immediate implication of this finding was that hubs needed be mapped at the individual level in our NIBS experiment. More broadly, it is notable that a group-average can fail to accurately represent salient topological features of individual brains. Thus, the practice of utilizing group-average derived regions-of-interest, either as NIBS targets or as nodes in network analyses, may be dubious in individuals.

### *Hubs can be mapped reliably within an individual*

To determine the quantity of rsfMRI data necessary for achieving high test-retest reliability of hub estimates, we randomly sampled non-overlapping epochs from each MSC participant's 5-hour rsfMRI time-series. Participation coefficients for right middle frontal gyrus parcels were calculated separately using each epoch, and reliability was quantified using rank spatial correlation. This procedure was repeated $10^3$ times per epoch, with epoch lengths ranging from 1 to 60 minutes (in 1-minute steps). The resultant time x reliability curves indicated low reliability when using typical amounts of fMRI data (i.e., 5-20 minutes) but higher reliability with additional data (see **Figure1f** for MSC01 and **FigureS1** for all participants). For example, we observed an average $r_s$ of 0.82 ± 0.10 when using 45-minutes of rsfMRI data. Thus, test-retest reliability of hub estimates is high when utilizing large amounts of per-individual data. For this reason, we collected 45-minutes of rsfMRI in the subsequent NIBS experiment.

### *Precision mapping and inhibitory stimulation of hubs*

Twenty-four healthy participants completed three visits of a prospective within-subjects double-blind experiment (**Figure2a**). Forty-five minutes of rsfMRI and a high-resolution anatomical image from the initial visit were submitted to an automated pipeline (**Figure2b**) that mapped a hub (as the highest-participation coefficient parcel) and non-hub (as the lowest-participation coefficient parcel ≥ 20mm from the hub) in the right middle frontal gyrus of each participant (**Figure2c**). The native-image space coordinates corresponding to the centroid of the hub and non-hub were then pseudo-randomly assigned as targets for two follow-up sessions (average interval between sessions = 5.8 ± 5.3 days). Immediately prior to performing an N-back fMRI task during both sessions, continuous theta burst stimulation (cTBS) [35] was administered offline, double-blind, and guided by neuronavigation. cTBS was best-suited for our investigation, as the aftereffects are thought to last up to fifty-minutes [36], long-enough to complete the twelve-minute N-back task. Notably, we determined post-hoc that hub and non-hub parcels did not significantly differ in their anatomical positioning, activation, or distance to the stimulating coil (**FigureS2**).

### *Hub inhibition slows information processing*

We quantified differences in N-back performance using a drift diffusion model (**Figure3a**), a well-validated computational model that is advantageous to considering response times and accuracy in isolation from one another [37]. This model takes as input the mean and variance of response times for correct trials, and mean accuracy and calculates cognitively-relevant latent variables indexing the speed and accuracy of information processing ("drift rate"), response conservativeness ("boundary separation"), and non-decision time. Of these three diffusion parameters, drift rate (**Figure3b**, "*v*") was most relevant for our predictions, as worse task performance manifests as slower drift rates (i.e., slower, more variable, less accurate performance).

A repeated measures 2x4 ANOVA (target x load) performed using drift rates revealed a main effect of target [$F(1,23)=8.87$, $p=0.005$], such that drift rates following cTBS to hubs were slower than those following cTBS to non-hubs (**Figure3c**). This finding demonstrates, as predicted, that hub inhibition impaired performance more so than non-hub inhibition. Notably, this effect remained in ANCOVA models where the difference in anatomical positioning, activation, network membership, and distance to TMS coil was included as a between participant covariate (**TableS1**). As expected, we also observed a main effect of load

[$F(1,23)=23.98$, $p<0.001$], confirming that higher cognitive loads were more difficult than lower loads. Load and cTBS target did not interact [$F(1,23)=0.07$, $p=0.79$]), indicating that the difference in drift rate following hub and non-hub cTBS did not vary by cognitive load.

ANOVA models were also performed on response boundary (**Figure3d**) and non-decision time (**Figure3e**) parameters. We observed main effects of load (response boundary: [$F(1,23)=22.37$, $p<0.001$]; non-decision time: [$F(1,23)=10.89$, $p<0.001$]), such that response conservativeness declined and non-decision time increased with higher N-back loads. However, there were no main effects of target (response boundary [$F(1,23)=1.21$, $p=0.27$]; non-decision time: [$F(1,23)=3.02$, $p=0.08$]) or target x load interactions (response boundary [$F(1,23)=0.003$, $p=0.96$]; non-decision time: [$F(1,23)=0.02$, $p=0.89$]). Thus, all three diffusion parameters were sensitive to cognitive load, and the effects of hub inhibition slowed drift rates, as predicted.

### *Hubs can be partitioned into discrete subtypes*

We predicted post-hoc that the effects of hub inhibition might have varied depending on which sets of networks the targeted hub participated in. We tested this possibility in an exploratory analysis. Three hub subtypes were identified ($Q = 0.17$, $z$-score = 6.47) by clustering together hubs exhibiting similar profiles of cross-network connectivity (**Figure4a**). For example, the first subtype was distinguished by its participation in the cingulo-opercular, dorsal attention, and sensory-motor networks, whereas a third subtype participated more in the default mode, ventral attention, and salience networks (**Figure4b**). Next, we examined the change in drift rate associated with each hub subtype (**Figure4c**). Inhibition of the first hub subtype slowed drift rates more so than the other two [$t(22)=2.06$, $p=0.05$]. While this analysis is limited by few per-subtype instances, it nonetheless raises the intriguing possibility of targeting hubs bridging select networks.

## Discussion

We presented three findings in this investigation. First, hubs were unique to individuals but could be mapped reliably within an individual. Second, inhibition of hubs with cTBS impaired N-back performance relative to inhibition of nearby non-hubs. Third, hubs could be clustered retrospectively into subtypes linking discrete sets of brain networks, which yielded different outcomes when inhibited. The broader implications of these points are considered further below.

### *Implications for neuroimaging individuals*

Our analysis of the MSC dataset challenged two common neuroimaging practices, and held critical implications for the design of neuroimaging experiments, including the present NIBS experiment. First, the spatial positioning of hubs was not similar across participants, and that a group-average map was an inaccurate representation of hubs in some individuals. Thus, the practice of using a group-average map (e.g., [24, 25]) to infer whether a given brain area functions as a hub in an individual [27, 38] is dubious. Second, hub estimates were unreliable when mapped with commonly utilized amounts of per-individual rsfMRI data. This finding is not entirely surprising given the low signal-to-noise ratio in BOLD fMRI data [39], and previous reports that small quantities of per-individual data fail to accurately characterize functional brain organization [17, 40, 41]. Our solution to these challenges was to map hubs in each individual using a large quantity of per-individual data, which yielded reliable hub estimates. High test-retest reliability was notable, as it suggests that inter-individual variability was neurobiologically meaningful, not noise. Gordon and colleagues [17] reported that whole-brain participation

coefficient estimates less reliable, regardless of how much per-individual data is utilized. Our analysis, in contrast, was constrained to right middle frontal gyrus. Thus, the test-retest reliability of network metrics may differ between anatomical regions, a possibility that should be investigated in future work.

### *Implications for network neuroscience*

Network science is a powerful and widespread conceptual framework in neuroscience [42, 43]. This approach distills the complexity of the brain into simple mathematical representations [21], which in turn allows one to form and test tractable hypotheses. It is critical, however, to validate the predictions of any conceptual framework against known variables. For example, if the importance of a node for network functioning can indeed be inferred from its topological positioning, then hub brain areas should serve outsized roles [24, 44, 45]. To date, evidence supporting this prediction has been either been correlational [25, 46, 47] or lesion-based [27, 38], both of which have limited interpretability. Here, we tested this prediction directly by precisely mapping hubs in individuals and temporarily inhibiting them with cTBS. Our finding that hub inhibition slowed information processing more than non-hub inhibition is conclusive evidence that hubs mapped using rsfMRI represent causal linchpins underlying cognition – not epiphenomena.

Which sets of networks a hub node participates in may be as critical to understanding the role of that node in a network as its generic status as a hub. There is no consensus, however, regarding the functions performed by many brain networks, making a purely hodological approach to estimating hub roles difficult [24]. For this reason, we did not attempt to map hubs participating in specific sets of networks a priori. Hubs were instead clustered post-hoc, and the relevance of each resultant subtype for N-back performance assessed objectively based on the change in drift rate following inhibition with cTBS. Information processing was slowed the most by inhibiting the hub subtype distinguished by its participation in select control (cingulo-opercular [48-50] and dorsal attention [51]) and sensory-motor networks (visual and dorsal somatosensory) networks. Interestingly, this subtype was weakly affiliated with the fronto-parietal network which, given its role in higher-order cognition [49], might have been predicted a priori as the network most critical for performing an N-back task. This finding is consistent, however, with the hypothesis that hubs serve outsized roles because they facilitate interactions between sets of networks [45], and not due to their affiliation with any single network (see **TableS2**). The specific subtypes identified in this investigation should be considered preliminary, however, as we only clustered hubs in located in right middle frontal gyrus, and additional work on this topic is warranted.

### *Interpreting diffusion model parameters*

The computational model applied in our investigation assumes an accumulation of noisy information supporting a decision process - whether or not the current stimulus matches one occurring *N*-trials ago. Conceptually, drift rate indexes the average rate at which this information accumulates, and in practice, faster drift rates manifest as faster, less variable response times and more correct responses. Thus, slower drift rates indicate an impairment in performance, whereas instructions that emphasize speed at the expense of accuracy reduce the response boundary parameter [52, 53]. For this reason, we predicted that hub inhibition would slow drift rates.

Slower drift rates may indicate a disruption in the accumulation and transfer of task-relevant information distributed amongst brain networks bridged by the hub. Although

speculative, such a scenario could account for why inhibiting one hub subtype slowed drift rates more than the others (i.e., if task-relevant information was present in networks associated with that hub subtype more than others). As an analogy, two international airports (i.e., hubs) can both serve critical roles in facilitating air travel, but a disruption in one can impede travel between some countries (i.e., modules) more so than others.

Although one might have predicted that hub inhibition would slow drift rates more during higher cognitive loads, as cross-network connectivity increases linearly with cognitive load [54, 55], we did not observe such an interaction. One potential explanation is that hub inhibition led to a different route of information transfer between brain networks, which was less efficient by a fixed amount, regardless of cognitive load. Finally, while our data cannot address whether our findings would generalize to a different cognitive process, future work can test our prediction that excitation or inhibition of a hub will facilitate or inhibit performance to the extent that interactions between networks bridged by that hub are necessary.

### *Implications for clinical applications*

An effective stimulation site was mapped in individuals by applying areal-parcellation and network science techniques to rsfMRI data. Thus, our investigation is distinct from previous work reporting that N-back performance following TMS is different from a sham (i.e., placebo) condition [56, 57]. In contrast, we found that N-back performance following active stimulation of two areas differing only in their rsfMRI connectivity, and separated by only 3cm on average, nonetheless produced significantly different behavioral outcomes. This finding is compatible with an attractive hypothesis that variable outcomes in clinical NIBS interventions are due in part to functional heterogeneity within a prescribed gross anatomical target. For example, seminal work by Fox and colleagues has reported that connectivity between the stimulated area of dorsolateral prefrontal cortex and the subgenual cingulate predicts response in patients with depression [58, 59]. This previous work was retrospective and utilized group-averaged connectivity estimates from 1000 healthy individuals [60]. Whether the personalized, network-centric strategy presented here is advantageous is an important question for future work.

There is growing interest in using non-invasive neuroimaging to guide NIBS interventions [61, 62]. Thus, a critical next step will be to evaluate whether the strategy outlined in this investigation can improve the therapeutic efficacy of NIBS interventions. Key challenges will need to be considered first. For example, it is unlikely that any hub can serve as a transdiagnostic target. Instead, it may be necessary to target hubs that participate in specific sets of brain networks relevant for a patient's unique cognitive and behavioral deficits. This strategy is a major conceptual advance over targeting nodes of individual networks [58, 62], as hubs are positioned at the intersection of multiple networks, which affords an opportunity to modulate a wider range of symptoms. The ability to modulate multiple symptoms via hubs is appealing in populations with heterogeneous clinical profiles, such as depression [63]. For example, a hub participating in affective and control networks might be targeted in patients with self-referential processing and executive deficits, whereas a hub participating in networks supporting reward and motor functioning might be targeted for treating anhedonia and psychomotor retardation.

### *Conclusions*

The prevailing strategy in the field of human neuroimaging is to average rsfMRI data from a large group of individuals, which has proven effective for characterizing coarse, albeit reliable [60] and cognitively-relevant [64], features of functional brain organization. However,

this group-average approach obscures salient topological features unique to individuals [17], limiting its ability provide clinically actionable information. As a result, there is growing need to generate high-fidelity maps of individual brains [65, 66], and to establish which brain features may be clinically useful as sites for intervention. Here we validated hubs mapped in individuals using rsfMRI as causal linchpins serving outsized roles in cognition, and propose stimulating hubs participating in networks relevant for patient symptomatology as a novel intervention strategy.

## Methods

### Midnight Scan Club analyses

*Participants*

The Midnight Scan Club (MSC) dataset [17] was downloaded from OpenfMRI.org (ds000224). This dataset is comprised of ten participants aged 24-34 years (mean age = 29.1 years ± 3.3, 5F/5M) that underwent a total of 5-hours of rsfMRI (10x30 minutes, each session acquired at midnight on subsequent days). This dataset included previously generated individual-specific areal parcellations [19] and network structures [67]. In addition, a group-average areal-parcellation and network-structure was generated here to enable comparisons between individual-specific hub estimates and those derived using a group-average approach. Further details regarding data acquisition and sample demographics are reported by [17].

*Establishing the necessity and feasibility of mapping hubs in individuals*

Participation coefficients were calculated using each MSC participant's 5-hr. rsfMRI dataset, following the procedure outlined in the "Automated pipeline for identifying stimulation targets" section of this Methods section. To quantify the spatial variability of participation coefficients within right middle frontal gyrus amongst MSC participants, a matrix was constructed, where the entry *ij* denotes the similarity of participation coefficients in participant *i* relative to those in participant *j*. This analysis required comparing participation coefficients in participants with unique areal parcellations. In order to do so, a best match for each parcel in participant *i* was defined in participant *j* as the parcel with a centroid closest in geodesic space, similar to how individual-specific system patches were matched in [16]. Similarity of matched parcels was assessed using rank correlation. A second matrix was constructed, where entries denoted the distance in euclidean space between the Talairach coordinates corresponding to the centroid of the highest participation coefficient parcel in each individual's right middle frontal gyrus. Test-retest reliability of participation coefficients within each MSC participant was quantified in an iterative split-half analysis. Two sets of participation coefficient values were calculated using two epochs of rsfMRI data ranging from 1- to 60-minutes (in 1-minute steps). For each epoch, we randomly and iteratively ($10^3$ times) selected two equal sized, non-overlapping, and motion censored epochs of resting-state time-series data.

### Non-invasive brain stimulation experiment

*Participants*

Twenty-four participants aged 18-28 years (mean age = 20.5 years ± 2.5, 11F/13M) were recruited from the Georgetown community and completed three study sessions (average interval between sessions = 5.86 ± 5.34 days) after complying with the consenting guidelines of

the Georgetown University IRB. Participants were screened for history of neurologic and psychiatric conditions, epilepsy, contraindications for MRI, and use of medications that increase likelihood of side effects following TMS.

*Data acquisition*

All data was acquired on a Siemens Trio 3T with the participant's head immobilized using head cushions. A high resolution structural T1 scan was acquired with the following parameters: MPRAGE: TR/TE = 1900/2.52 ms, 90-degree flip angle, 176 sagittal slices with a 1.0 mm thickness. Functional echo-planar images were acquired with the following parameters during each imaging sessions: 3 mm isotropic resolution, TR = 2000 ms, TE = 30 ms, flip angle = 90°, FOV = 192 × 192 mm. A T1 and three resting-state runs, each lasting 15-minutes and acquired successively, were collected during the initial imaging visit. An N-back task consisting of 20 blocks (5 blocks each of 1-, 2-, 3-, and 4-back loads, in pseudo-randomized order) was administered during each study visit. N-back fMRI data was not analyzed for the purposes of this investigation. Blocks consisted of 9 letters, each presented for a duration of 500ms and with an inter-trial interval of 1500ms. Participants were instructed to provide a right-hand button press for targets (i.e., letters matching those presented *N*-trials ago) and a left-hand button press for non-targets (i.e., letters not matching those presented *N*-trials ago) as quickly and accurately as possible. Of the 180 trials, 32 were targets, and either one or two targets were in any given block. Stimuli were presented on a back-projection screen using the E-Prime software.

*Data preprocessing*

Functional images were corrected for differences in motion and slice timing acquisition, and co-registered into each participant's own high-resolution anatomical space using SPM12 (Wellcome Department of Cognitive Neurology, London, United Kingdom). Functional data was denoised using the *aCompCor* strategy in the CONN toolbox. Denoising steps included linear de-trending and nuisance regression (5 principle components from white matter and cerebrospinal fluid masks derived from an MPRAGE segmentation; 6 motion parameters and first-order temporal derivatives; and point-regressors to censor time points with mean frame-wise displacement > 0.2mm). Residual time-series were band-pass filtered (0.01 Hz < $f$ < 0.1 Hz). Temporal masks were created to flag motion-contaminated frames for scrubbing. Contaminated volumes were identified by frame-by-frame displacement (FD) calculated as the sum of absolute values of the differentials of the 3 translational motion parameters and 3 rotational motion parameters. On average, 76 ± 3% of the rsfMRI time-series was retained after performing motion censoring.

*Surface file generation*

Following volumetric co-registration, white and pial anatomical surfaces were generated from each participant's native-space MPRAGE using Freesurfer's recon-all pipeline (version 5.0). The fsaverage-registered left and right hemisphere surfaces were then brought into register with each other in fs_LR space [68] and resampled to a resolution of 32k vertices using Caret tools (http://brainvis.wustl.edu/wiki/index.php/Caret:Operations/Freesurfer_to_fs_LR). Denoised fMRI time-series within the cortical ribbon (those situated between the white and pial surfaces) were mapped onto each individual's midthickness surface (the average of the white and pial surfaces) and spatially smoothed (σ=2.55). Both left and right surfaces were combined into the Connectivity Informatics Technology Initiative (CIFTI) format using Connectome

Workbench [69], yielding time courses representative of the entire cortical surface, excluding non-gray matter tissue, and sub-cortical structures.

**Automated pipeline for identifying stimulation targets**

The following portion of the methods section details the steps applied to each participant's denoised rsfMRI CIFTI file from the baseline study visit. All of the steps below were performed as part of a single automated pipeline, allowing both the cTBS administrator (CJL) and participant to remain blinded.

*Boundary-based parcellation*

A boundary-based parcellation was generated by applying the procedures developed by [19] on each participant's resting-state CIFTI dataset. In a boundary map, boundaries represent transition points in whole-brain functional connectivity patterns along the cortical surface. Parcels were generated using the "watershed by flooding" procedure. Parcels smaller than 10 cortical vertices (~20mm$^2$) were removed. The number of resultant parcels varied between individuals (mean parcel count: 548, range: 473-603). Group-level parcellations yield fewer and larger parcels (e.g., 333 parcels in [19], 360 in [70]). The number of parcels reported here was judged to be biologically plausible, however, with consideration to recent work [41] estimating a similar number of parcels (616) in a highly-sampled individual brain.

*Network template-matching*

Calculation of participation coefficients requires a known community structure (i.e., a network affiliation for each node included in the calculation). Unsupervised clustering or community detection algorithms are often used to identify collections of nodes that comprise functional networks. This approach, however, can identify a variable number of networks across individuals or those with no clear functionality. In contrast, our goal was to match parcels with a common set of known functional brain networks. For this reason, we utilized the template matching procedure developed by [15], which matches each parcel to 1 of 12 canonical network templates generated in an independent sample of healthy adults (N=120) using the InfoMap algorithm [67]. We selected this approach as it assigns parcels to a common set of functional networks, which aids comparison amongst participants. **Supplementary FigureS3** includes the areal-parcellation and network structure for each participant.

*Identification of hub and non-hub cTBS targets*

The temporal correlation between each parcel and all other parcels was computed using the denoised motion-censored rsfMRI time-series, yielding a parcel X parcel functional connectivity matrix for each participant. Local connections (those < 20mm in geodesic space) were eliminated, to avoid local blurring of signals between adjacent parcels. The participation coefficient and nodal degree was calculated for each parcel. To do so, we first calculated ten participation coefficients and degree values for each parcel using binarized functional connectivity matrices, each with a unique density (1-10%, in 1% steps). The final participation coefficient and degree for each parcel was the average of these ten values. Participation coefficient was calculated using the equation below, where $M$ is the total set of networks, $k_i$ is the number of edges associated with node $i$, and $k_i(m)$ is the number of edges between node $i$ and all nodes in network $m$.

$$P_i = 1 - \sum_{m \in M} \left( \frac{K_i(m)}{K_i} \right)^2$$

Native-space MPRAGE coordinates corresponding to the centroid of a hub and non-hub parcel in each participant's right middle frontal gyrus were identified using the following procedure. First, as the participation coefficient of a parcel with few connections is dubious, we eliminated from consideration parcels with a degree in the bottom quartile of whole-brain values. Remaining parcels with a centroid falling within right middle frontal gyrus, defined using Freesurfer gyral labels, were identified. The hub was defined as the right middle frontal gyrus parcel with the highest participation coefficient value. Next, the euclidean distance between the hub and all other parcels in right middle frontal gyrus was calculated. The non-hub was defined as the parcel with the lowest participation coefficient value >20mm from the centroid of the hub parcel in euclidean space. This minimum distance was enforced to enable selective targeting of the two parcels, given evidence that the spatial resolution of TMS is 0.5-2cm [32-34]. Native-space MPRAGE coordinates corresponding to the hub or non-hub centroid were pseudo-randomly assigned as the stimulation sites for the two follow-up sessions.

*Continuous theta-burst stimulation and MRI-guided neuronavigation*

cTBS was applied using a MagPro x100 device (MagVenture, Inc., Atlanta, GA) with a passively coiled MCF-B70 figure 8 coil. cTBS is a safe [71] and inhibitory form of patterned TMS involving three 50Hz pulses in trains repeated at 200-ms intervals [35]. cTBS was administered in a room adjacent to a "ready-to-scan" magnet environment (i.e., MRI-safety questionnaire completed, scanner console & E-prime set-up prepared), which minimized the delay between cTBS administration and task performance. Parcel centroids were targeted using the Brainsight 2 Frameless stereotactic system for image guided TMS research (Rogue Research, Montreal, Canada). This system uses infrared reflectors attached to a headband worn by the subject to co-register the MPRAGE with the participant's head. The stimulating coil was similarly co-registered via infrared reflectors allowing for precise control of the stimulation site. Each participant's active motor threshold was defined as the intensity required to induce a motor evoked potential in the contralateral FDI muscle when pulses were applied to right motor cortex during a mild sustained contraction. The stimulus intensity was 80% of active motor threshold. Muscle twitches were measured using surface electrodes placed on the FDI muscle, which are connected to an electromyography device incorporated into the BrainSight system. During cTBS, the parcel was delineated on the subject's native MPRAGE.

**Drift diffusion modeling of task performance**

A drift diffusion model was utilized to quantify task performance. We selected an EZ-diffusion model [37], in place of alternative diffusion fitting routines, as it is more effective in resolving individual differences in parameter values [53] and does not require characterizing the distribution of incorrect response times, making it well-suited for use in populations where the error rate is relatively low. A 2x4 (target x load) repeated measure ANOVA was performed on each of three diffusion model parameters - drift rate, boundary separation, and non-decision time. Tables containing summary statistics for accuracy and response times can be found in the **Supplementary Tables S3** & **S4**.

### Partitioning hubs into subtypes

The percentage of hub edges to each network module was calculated for each participant (number of edges with network *i* divided by nodal degree) across a range of graph densities (1-10%, in 1% steps). A correlation matrix was then generated, where the entry *ij* indicated the degree to which the distribution of edges amongst network modules was correlated in participants *i* and *j*. The Louvain community detection algorithm [21] was applied to this weighted, signed correlation matrix $10^3$ times, and a consensus partition generated using an association-recluster strategy [72]. In an association-recluster framework, modularity maximization identifies a consensus partition from an association matrix, where entries denote the frequency with which nodes co-occur in a community across iterations. The significance of this consensus partition was quantified as a *z*-score, by comparing the associated modularity function ("Q") against a null distribution ($10^3$ iterations) of *Q* values derived from random graphs with preserved signed degree distributions [73].

## Figure Captions

**Figure1** – Establishing the necessity and feasibility of high-fidelity hub mapping in individuals. Hub nodes participate in more network modules, and have a high participation coefficient, whereas non-hub hub nodes participate in fewer network modules, and have a low participation coefficient (**a**). A participation coefficient was calculated for each parcel in the right middle frontal gyrus of the highly-sampled MSC participants (**b**). Inter-individual variability in spatial distribution of participation coefficients (**c**) and distance in euclidean space between the highest participation coefficient parcel in each participant was summarized in matrices (**d**). Distances between individual-specific hubs and the group-average ("G") hub. Red line represents an estimated spatial resolution of TMS (**e**). Test-retest reliability of hub estimates within individuals improves with greater quantities of per-individual data (**f**).

**Figure2** – A prospective, within-subjects, double-blind experimental design to test if hubs serve outsized roles in cognition (**a**). 45-minutes of rsfMRI and a high-resolution structural image collected during an initial study visit was submitted to an automated pipeline (**b**). Major pipeline steps include the construction of an individual-specific areal parcellation (red denotes boundaries between functional areas) and network structure (colors denote unique networks), and sparse functional connectivity matrices (a spring graph with a density of 1% for visualization). Participation coefficients for parcels with a centroid in right middle frontal gyrus were calculated. Parcels with the highest ("hub") and lowest ("non-hub") participation coefficients were pseudo-randomly assigned as targets for follow-up sessions [**c**: hubs (red) and non-hub (gray) cTBS targets in nine representative participants]. DMN = default mode network, VIS = visual, FP = fronto-parietal, DAN = dorsal attention network, SAL = salience, VAN = ventral attention, AUD = auditory, dSM = dorsal somatosensory, vSM = ventral somatosensory, mPar = medial parietal, PO = parieto-occipital, COP = cingulo-opercular.

**Figure3** – Drift diffusion modeling of N-back performance following hub and non-hub inhibition with cTBS. The drift diffusion model (**a**) takes as input the variance and mean response time for correct trials and the mean accuracy for each cognitive load and calculates latent variables representing the speed of information processing or drift rate ("v"), response conservativeness ("a"), and the amount of time unrelated to the decision process ("ter"). Correlation matrix, where entries denote the pairwise relationships amongst input and output drift diffusion model parameters using Pearson correlation (**b**). Hub cTBS slowed drift rates across N-back loads, relative to non-hub cTBS (**c**), but did not have an effect on response-boundary (**d**) or non-decision time (**e**). Gray bars = non-hub inhibition, red bars = hub inhibition.

**Figure4** – Hubs can be clustered into subtypes (**a**) that participate in discrete sets of network modules (**b**). Average change in drift rate (vs. non-hub inhibition) following inhibition of each hub subtype (**c**). DMN = default mode network, VIS = visual, FP = fronto-parietal, DAN = dorsal attention network, SAL = salience, VAN = ventral attention, AUD = auditory, dSM = dorsal somatosensory, vSM = ventral somatosensory, mPar = medial parietal, PO = parieto-occipital, COP = cingulo-opercular.

## References


1. Guo, Q., C. Li, and J. Wang, *Updated Review on the Clinical Use of Repetitive Transcranial Magnetic Stimulation in Psychiatric Disorders.* Neurosci Bull, 2017.
2. Salling, M.C. and D. Martinez, *Brain Stimulation in Addiction.* Neuropsychopharmacology, 2016. **41**(12): p. 2798-2809.
3. Diana, M., et al., *Rehabilitating the addicted brain with transcranial magnetic stimulation.* Nat Rev Neurosci, 2017. **18**(11): p. 685-693.
4. Bais, M., M. Figee, and D. Denys, *Neuromodulation in obsessive-compulsive disorder.* Psychiatr Clin North Am, 2014. **37**(3): p. 393-413.
5. Val-Laillet, D., et al., *Neuroimaging and neuromodulation approaches to study eating behavior and prevent and treat eating disorders and obesity.* Neuroimage Clin, 2015. **8**: p. 1-31.
6. Edwardson, M.A., et al., *New modalities of brain stimulation for stroke rehabilitation.* Exp Brain Res, 2013. **224**(3): p. 335-58.
7. George, M.S., et al., *Daily left prefrontal transcranial magnetic stimulation therapy for major depressive disorder: a sham-controlled randomized trial.* Arch Gen Psychiatry, 2010. **67**(5): p. 507-16.
8. Avissar, M., et al., *Functional connectivity of the left DLPFC to striatum predicts treatment response of depression to TMS.* Brain Stimul, 2017. **10**(5): p. 919-925.
9. Gaynes, B.N., et al., *Repetitive transcranial magnetic stimulation for treatment-resistant depression: a systematic review and meta-analysis.* J Clin Psychiatry, 2014. **75**(5): p. 477-89; quiz 489.
10. Fox, M.D., et al., *Measuring and manipulating brain connectivity with resting state functional connectivity magnetic resonance imaging (fcMRI) and transcranial magnetic stimulation (TMS).* Neuroimage, 2012. **62**(4): p. 2232-43.
11. Pascual-Leone, A., et al., *Rapid-rate transcranial magnetic stimulation of left dorsolateral prefrontal cortex in drug-resistant depression.* Lancet, 1996. **348**(9022): p. 233-7.
12. Fitzgerald, P.B., et al., *A randomized trial of rTMS targeted with MRI based neuro-navigation in treatment-resistant depression.* Neuropsychopharmacology, 2009. **34**(5): p. 1255-62.
13. Sack, A.T., et al., *Optimizing functional accuracy of TMS in cognitive studies: a comparison of methods.* J Cogn Neurosci, 2009. **21**(2): p. 207-21.
14. Mueller, S., et al., *Individual variability in functional connectivity architecture of the human brain.* Neuron, 2013. **77**(3): p. 586-95.
15. Gordon, E.M., et al., *Individual Variability of the System-Level Organization of the Human Brain.* Cereb Cortex, 2015.
16. Gordon, E.M., et al., *Individual-specific features of brain systems identified with resting state functional correlations.* Neuroimage, 2016.
17. Gordon, E.M., et al., *Precision Functional Mapping of Individual Human Brains.* Neuron, 2017.

18. Cohen, A.L., et al., *Defining functional areas in individual human brains using resting functional connectivity MRI.* Neuroimage, 2008. **41**(1): p. 45-57.
19. Gordon, E.M., et al., *Generation and Evaluation of a Cortical Area Parcellation from Resting-State Correlations.* Cereb Cortex, 2014.
20. Wang, D., et al., *Parcellating cortical functional networks in individuals.* Nat Neurosci, 2015. **18**(12): p. 1853-60.
21. Rubinov, M. and O. Sporns, *Complex network measures of brain connectivity: uses and interpretations.* Neuroimage, 2010. **52**(3): p. 1059-69.
22. Guimera, R. and L.A. Amaral, *Cartography of complex networks: modules and universal roles.* J Stat Mech, 2005. **2005**(P02001): p. nihpa35573.
23. Jeong, H., et al., *Lethality and centrality in protein networks.* Nature, 2001. **411**(6833): p. 41-2.
24. Power, J.D., et al., *Evidence for hubs in human functional brain networks.* Neuron, 2013. **79**(4): p. 798-813.
25. Bertolero, M.A., B.T. Yeo, and M. D'Esposito, *The modular and integrative functional architecture of the human brain.* Proc Natl Acad Sci U S A, 2015. **112**(49): p. E6798-807.
26. Sporns, O. and ebrary Inc., *Networks of the brain*. 2011, MIT Press: Cambridge, Mass.
27. Warren, D.E., et al., *Network measures predict neuropsychological outcome after brain injury.* Proc Natl Acad Sci U S A, 2014. **111**(39): p. 14247-52.
28. Fornito, A., A. Zalesky, and M. Breakspear, *The connectomics of brain disorders.* Nat Rev Neurosci, 2015. **16**(3): p. 159-72.
29. Baddeley, A., *Working memory.* Curr Biol, 2010. **20**(4): p. R136-40.
30. Owen, A.M., et al., *N-back working memory paradigm: a meta-analysis of normative functional neuroimaging studies.* Hum Brain Mapp, 2005. **25**(1): p. 46-59.
31. Guimera, R. and L.A. Nunes Amaral, *Functional cartography of complex metabolic networks.* Nature, 2005. **433**(7028): p. 895-900.
32. Brasil-Neto, J.P., et al., *Optimal focal transcranial magnetic activation of the human motor cortex: effects of coil orientation, shape of the induced current pulse, and stimulus intensity.* J Clin Neurophysiol, 1992. **9**(1): p. 132-6.
33. Wassermann, E.M., et al., *Noninvasive mapping of muscle representations in human motor cortex.* Electroencephalogr Clin Neurophysiol, 1992. **85**(1): p. 1-8.
34. Thielscher, A. and T. Kammer, *Linking physics with physiology in TMS: a sphere field model to determine the cortical stimulation site in TMS.* Neuroimage, 2002. **17**(3): p. 1117-30.
35. Huang, Y.Z., et al., *Theta burst stimulation of the human motor cortex.* Neuron, 2005. **45**(2): p. 201-6.
36. Wischnewski, M. and D.J. Schutter, *Efficacy and Time Course of Theta Burst Stimulation in Healthy Humans.* Brain Stimul, 2015. **8**(4): p. 685-92.
37. Wagenmakers, E.J., H.L. van der Maas, and R.P. Grasman, *An EZ-diffusion model for response time and accuracy.* Psychon Bull Rev, 2007. **14**(1): p. 3-22.
38. Gratton, C., et al., *Focal brain lesions to critical locations cause widespread disruption of the modular organization of the brain.* J Cogn Neurosci, 2012. **24**(6): p. 1275-85.
39. Welvaert, M. and Y. Rosseel, *On the definition of signal-to-noise ratio and contrast-to-noise ratio for FMRI data.* PLoS One, 2013. **8**(11): p. e77089.
40. Anderson, J.S., et al., *Reproducibility of single-subject functional connectivity measurements.* AJNR Am J Neuroradiol, 2011. **32**(3): p. 548-55.
41. Laumann, T.O., et al., *Functional System and Areal Organization of a Highly Sampled Individual Human Brain.* Neuron, 2015. **87**(3): p. 657-70.
42. Medaglia, J.D., M.E. Lynall, and D.S. Bassett, *Cognitive network neuroscience.* J Cogn Neurosci, 2015. **27**(8): p. 1471-91.

43. Bassett, D.S. and O. Sporns, *Network neuroscience.* Nat Neurosci, 2017. **20**(3): p. 353-364.
44. van den Heuvel, M.P. and O. Sporns, *Network hubs in the human brain.* Trends Cogn Sci, 2013. **17**(12): p. 683-96.
45. Gratton, C., H. Sun, and S.E. Petersen, *Control networks and hubs.* Psychophysiology, 2017.
46. Cole, M.W., et al., *Multi-task connectivity reveals flexible hubs for adaptive task control.* Nat Neurosci, 2013. **16**(9): p. 1348-55.
47. Yeo, B.T., et al., *Functional Specialization and Flexibility in Human Association Cortex.* Cereb Cortex, 2014.
48. Dosenbach, N.U., et al., *A dual-networks architecture of top-down control.* Trends Cogn Sci, 2008. **12**(3): p. 99-105.
49. Dosenbach, N.U., et al., *Distinct brain networks for adaptive and stable task control in humans.* Proc Natl Acad Sci U S A, 2007. **104**(26): p. 11073-8.
50. Dosenbach, N.U.F., et al., *A Core System for the Implementation of Task Sets.* Neuron, 2006. **50**(5): p. 799-812.
51. Corbetta, M. and G.L. Shulman, *Control of goal-directed and stimulus-driven attention in the brain.* Nat Rev Neurosci, 2002. **3**(3): p. 201-15.
52. Ratcliff, R. and G. McKoon, *The diffusion decision model: theory and data for two-choice decision tasks.* Neural Comput, 2008. **20**(4): p. 873-922.
53. van Ravenzwaaij, D., C. Donkin, and J. Vandekerckhove, *The EZ diffusion model provides a powerful test of simple empirical effects.* Psychon Bull Rev, 2017. **24**(2): p. 547-556.
54. Cohen, J.R. and M. D'Esposito, *The Segregation and Integration of Distinct Brain Networks and Their Relationship to Cognition.* J Neurosci, 2016. **36**(48): p. 12083-12094.
55. Liang, X., et al., *Topologically Reorganized Connectivity Architecture of Default-Mode, Executive-Control, and Salience Networks across Working Memory Task Loads.* Cereb Cortex, 2016. **26**(4): p. 1501-11.
56. Schicktanz, N., et al., *Continuous theta burst stimulation over the left dorsolateral prefrontal cortex decreases medium load working memory performance in healthy humans.* PLoS One, 2015. **10**(3): p. e0120640.
57. Hoy, K.E., et al., *Enhancement of Working Memory and Task-Related Oscillatory Activity Following Intermittent Theta Burst Stimulation in Healthy Controls.* Cereb Cortex, 2016. **26**(12): p. 4563-4573.
58. Fox, M.D., et al., *Efficacy of transcranial magnetic stimulation targets for depression is related to intrinsic functional connectivity with the subgenual cingulate.* Biol Psychiatry, 2012. **72**(7): p. 595-603.
59. Weigand, A., et al., *Prospective Validation That Subgenual Connectivity Predicts Antidepressant Efficacy of Transcranial Magnetic Stimulation Sites.* Biol Psychiatry, 2017.
60. Yeo, B.T., et al., *The organization of the human cerebral cortex estimated by intrinsic functional connectivity.* J Neurophysiol, 2011. **106**(3): p. 1125-65.
61. Fischer, A.S., Keller, C.J., Etkin A., *The Clinical Applicability of Functional Connectivity in Depression: Pathways Toward More Targeted Intervention.* Biological Psychiatry: Cognitive Neuroscience and Neuroimaging 2016.
62. Dubin, M.J., et al., *Network-Guided Transcranial Magnetic Stimulation for Depression.* Curr Behav Neurosci Rep, 2017. **4**(1): p. 70-77.
63. Drysdale, A.T., et al., *Resting-state connectivity biomarkers define neurophysiological subtypes of depression.* Nat Med, 2017. **23**(1): p. 28-38.

64. Smith, S.M., et al., *Correspondence of the brain's functional architecture during activation and rest.* Proc Natl Acad Sci U S A, 2009. **106**(31): p. 13040-5.
65. Finn, E.S., et al., *Functional connectome fingerprinting: identifying individuals using patterns of brain connectivity.* Nat Neurosci, 2015. **18**(11): p. 1664-71.
66. Poldrack, R.A., *Precision Neuroscience: Dense Sampling of Individual Brains.* Neuron, 2017. **95**(4): p. 727-729.
67. Rosvall, M. and C.T. Bergstrom, *Maps of random walks on complex networks reveal community structure.* Proc Natl Acad Sci U S A, 2008. **105**(4): p. 1118-23.
68. Van Essen, D.C., et al., *Parcellations and hemispheric asymmetries of human cerebral cortex analyzed on surface-based atlases.* Cereb Cortex, 2012. **22**(10): p. 2241-62.
69. Glasser, M.F., et al., *The minimal preprocessing pipelines for the Human Connectome Project.* Neuroimage, 2013. **80**: p. 105-24.
70. Glasser, M.F., et al., *A multi-modal parcellation of human cerebral cortex.* Nature, 2016. **536**(7615): p. 171-8.
71. Oberman, L., et al., *Safety of theta burst transcranial magnetic stimulation: a systematic review of the literature.* J Clin Neurophysiol, 2011. **28**(1): p. 67-74.
72. Betzel, R.F. and D.S. Bassett, *Multi-scale brain networks.* Neuroimage, 2016.
73. Maslov, S. and K. Sneppen, *Specificity and stability in topology of protein networks.* Science, 2002. **296**(5569): p. 910-3.

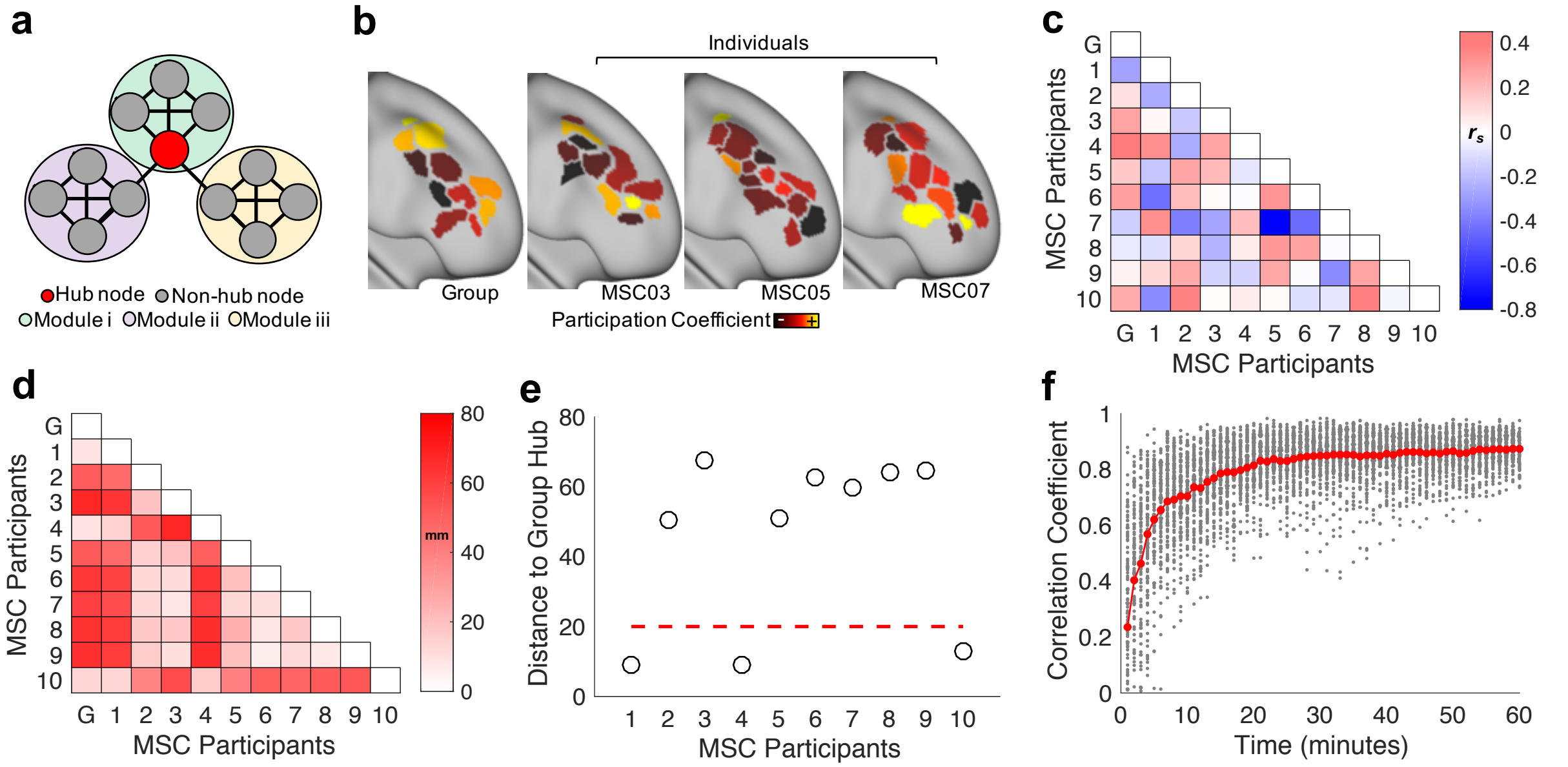
a
Hub node
Non-hub node
Module i
Module ii
Module iii
b
Individuals
Group
MSC03
MSC05
MSC07
Participation Coefficient
c
MSC Participants
$r_s$
0.4
0.2
0
-0.2
-0.4
-0.6
-0.8
d
MSC Participants
mm
80
60
40
20
0
e
Distance to Group Hub
MSC Participants
f
Correlation Coefficient
Time (minutes)

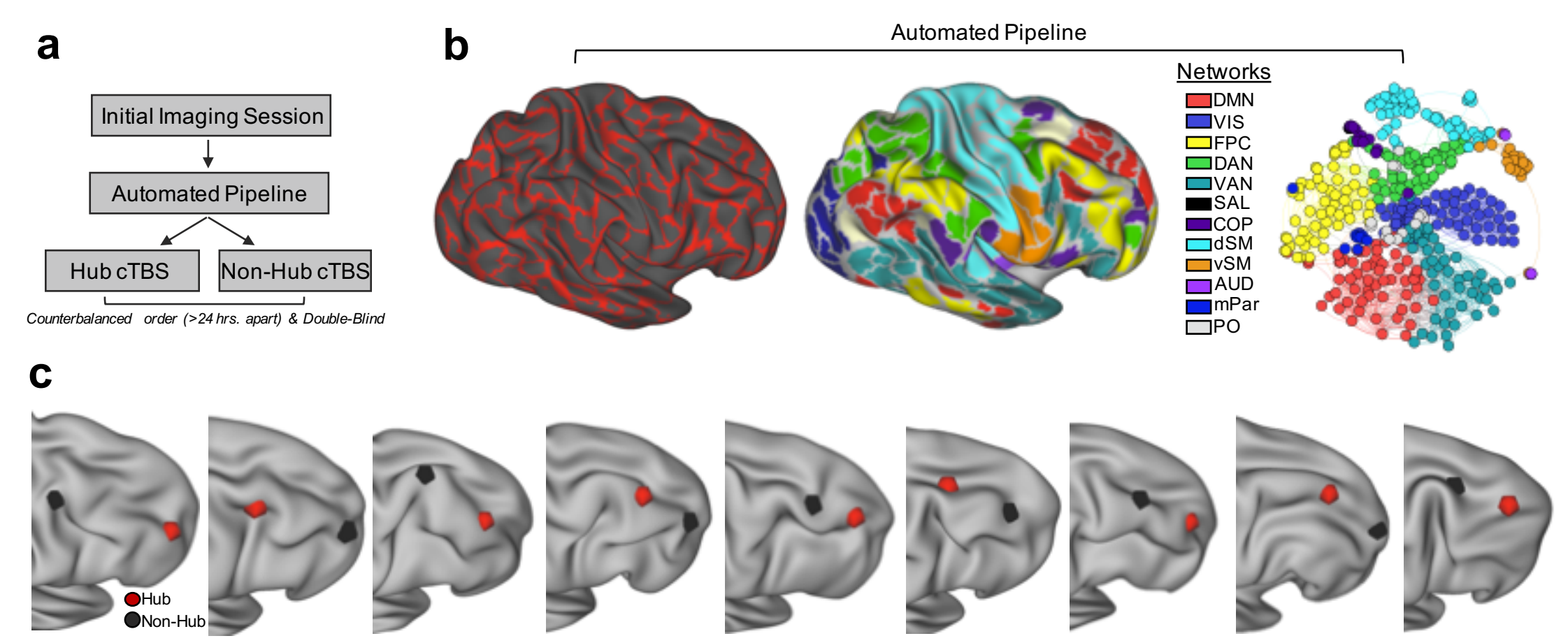
a
Initial Imaging Session
Automated Pipeline
Hub cTBS
Non-Hub cTBS
Counterbalanced order (>24 hrs. apart) & Double-Blind
b
Automated Pipeline
Networks
DMN
VIS
FPC
DAN
VAN
SAL
COP
dSM
vSM
AUD
mPar
PO
c
Hub
Non-Hub

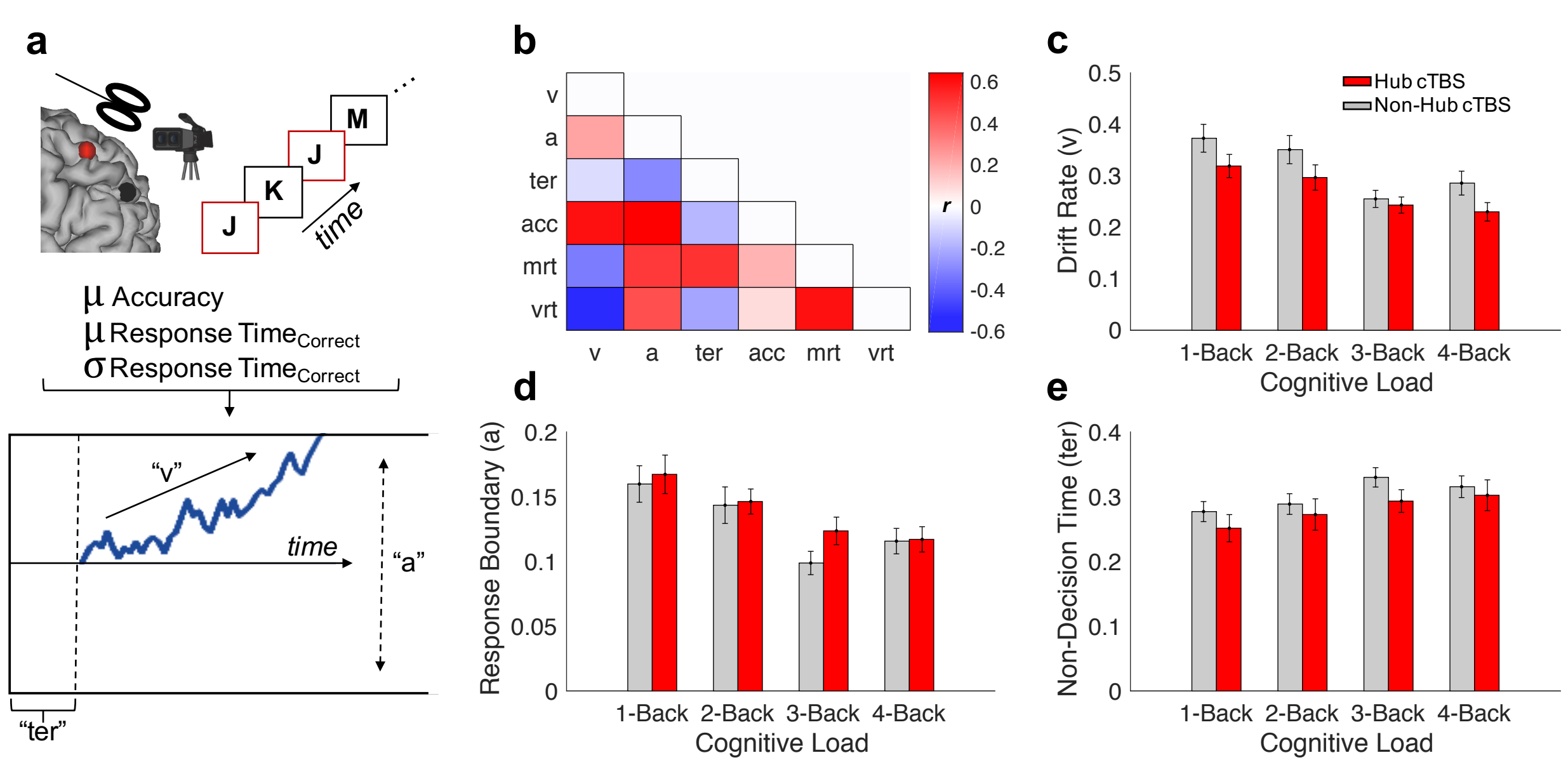
a
M
J
K
J
time
μ Accuracy
μ Response Time$_{Correct}$
σ Response Time$_{Correct}$
"v"
time
"a"
"ter"
b
v
a
ter
acc
mrt
vrt
r
0.6
0.4
0.2
0
-0.2
-0.4
-0.6
c
Hub cTBS
Non-Hub cTBS
Drift Rate (v)
0.5
0.4
0.3
0.2
0.1
0
1-Back
2-Back
3-Back
4-Back
Cognitive Load
d
Response Boundary (a)
0.2
0.15
0.1
0.05
0
1-Back
2-Back
3-Back
4-Back
Cognitive Load
e
Non-Decision Time (ter)
0.4
0.3
0.2
0.1
0
1-Back
2-Back
3-Back
4-Back
Cognitive Load

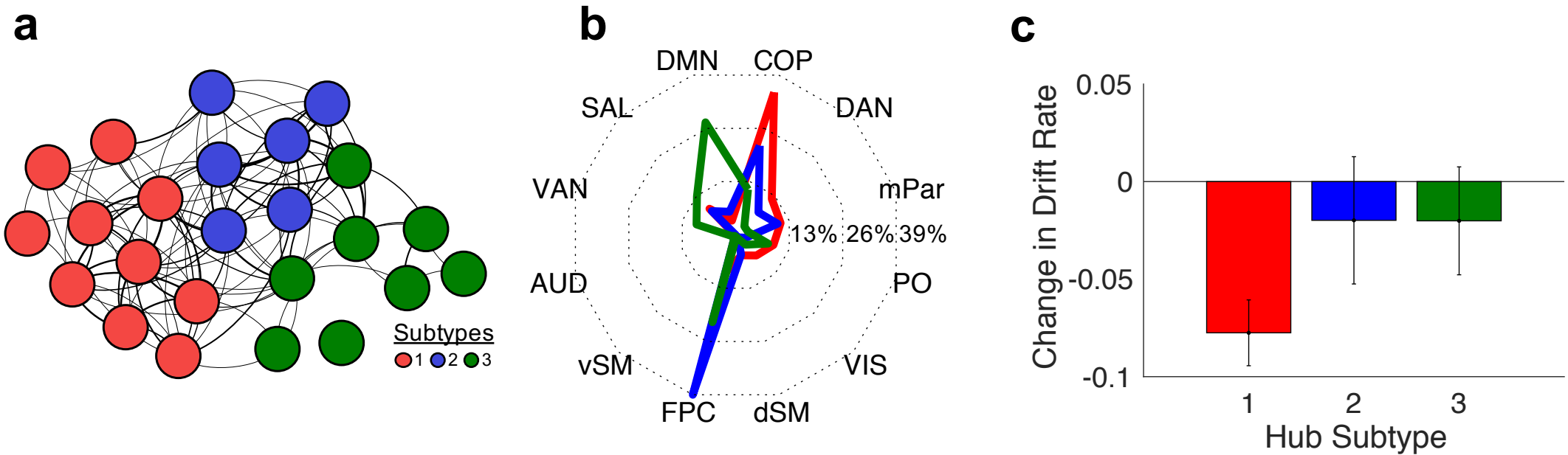
a
Subtypes
1 2 3
b
DMN
COP
DAN
mPar
PO
VIS
dSM
FPC
vSM
AUD
VAN
SAL
13%
26%
39%
c
Change in Drift Rate
0.05
0
-0.05
-0.1
1
2
3
Hub Subtype